International Conference on Mechanical, Industrial and Materials Engineering 2015 (ICMIME2015)
11-13 December, 2015, RUET, Rajshahi, Bangladesh.

Paper ID: FM-15

Thrust Produced by Four Fingers of a Swimmer at a Low Re

Md. Mahbub Alam[1], Guoqing Xu[1], Kerry Hourigan[2], Shafiqur Rehman[3]

[1]Institute for Turbulence-Noise-Vibration Interaction and Control, Shenzhen Graduate School, Harbin Institute of Technology, Shenzhen Graduate School, Shenzhen, China
[2]Fluids Laboratory for Aeronautical and Industrial Research (FLAIR), Department of Mechanical and Aerospace Engineering, Monash University, Clayton 3800, Australia
[3]Center for Engineering Research, Research Institute, King Fahd University of Petroleum and Minerals, Dhahran-31261, Saudi Arabia

E-mail: alamm28@yahoo.com; alam@hitsz.edu.cn

Abstract

Thrust produced by a swimmer might be connected the spacing between the four fingers. It is thus crucial to examine fluid dynamics around four side-by-side fingers. Flow structure and fluid forces acting on four identical side-by-side circular cylinders placed normal to the oncoming flow is numerically simulated using the finite volume method (FVM) at a low Reynolds number Re = 100, based on cylinder diameter D and freestream velocity. How the wake structure, forces and vortex shedding patterns are contingent on the cylinder gap spacing ratio g^* (= g/D) between the cylinders is studied systemically when g^* varies from 0 to 2. Based on the intrinsic features of the flow, four distinct flow regimes are identified in the range of g^* examined. The total time-mean drag force acting on the four cylinders escalates exponentially with a decrease in g^*, as does the lift force, repulsive, on each cylinder.

Keywords: drag force, four fingers, cylinders, swimmer, flow, wake.

1. Introduction

A large portion of forward thrust of a swimmer comes from palm and fingers. Propulsive forces generated by swimmers' palm/fingers should also be studied to find the optimum spacing between the fingers. Two side-by-side circular cylinders are considered as the simplest model to understand the fluid dynamics around more structures in groups. Alam et al. [1] experimentally investigated the aerodynamics of two side-by-side circular cylinders at a Reynolds number of 5.5×10^4, identifying four distinct flows depending on the gap spacing between the cylinders. The flows were distinguished not only by their structures, but also by shedding frequencies and fluid forces.

While a number of similar studies have been carried out for two circular cylinders in side-by-side arrangement, quite less attention has been paid to examine the fluid dynamics around more than two cylinders, where much more complex flow is involved. Some features of flow around multiple cylinders can be predicted based on the fluid dynamics knowledge of two cylinders but some are not, requiring investigation on more than two cylinders.

The objective of this investigation is to study the hydrodynamics of and drag forces acting four cylinders representing the four fingers of a hand at a low $Re = 100$.

2. Computation

Unsteady two-dimensional laminar flow of viscous incompressible fluid is considered. The finite volume method (FVM) with a structured quadrangular grid is employed to solve the unsteady two-dimensional incompressible Navier-Stokes equations. The dimensionless 2-D Navier-Stokes equations governing the flow of a Newtonian fluid can be written in vector form as

$$\left.\begin{aligned} \frac{\partial \boldsymbol{u}}{\partial t} + \boldsymbol{u}\cdot\nabla\boldsymbol{u} &= -\nabla p + \frac{1}{Re}\nabla^2\boldsymbol{u} \\ \nabla\cdot\boldsymbol{u} &= 0 \end{aligned}\right\} \qquad (1)$$

where $\boldsymbol{u}$ is the non-dimensional flow velocity vector in the Cartesian coordinate system (x, y) with its two velocity components u_1 and u_2; the dimensionless static pressure is denoted by p; Re is the Reynolds number based on the free-stream velocity U_0 and cylinder diameter D. The Re is is kept constant at Re = 100.

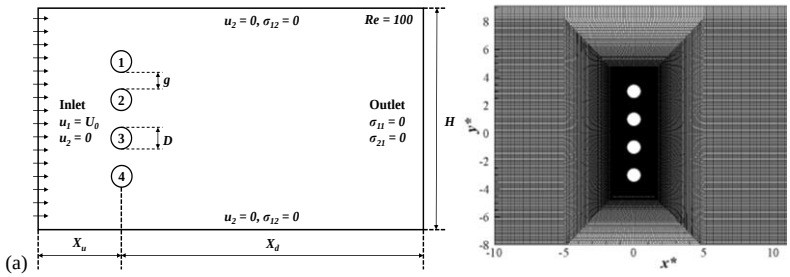

Fig. 1 (a) Computational domain, boundary conditions and symbol definitions, (b) grid system around the cylinders.

Fig. 1(a) shows a schematic diagram of the computation domain, cylinder arrangement, definitions of symbols and boundary conditions. The gap width between the cylinders is defined by g, normalized as $g^* = g/D$. An appropriate computational size of $X_u = 10D$, $X_d = 25D$ and $H = 80D$ is chosen, giving a converged output (Fig. 1). An O-xy grid system near the cylinders and a rectangular-grid system away from the cylinders were used (Fig. 1b). The number of grids for the O-grid system was 200 in the transverse direction. Therefore, a total of 200 points were on the cylinder surface. The grid in the radial direction was denser near the cylinder surface with the nearest grid being $0.005D$ away from the cylinder surface. On lateral surfaces, the velocity component normal to the boundaries and the stress vector component along the boundaries are set to zero. The no-slip boundary condition is applied at the cylinder walls. All simulations start with the initial velocity $u_1 = U_0$, $u_2 = 0$. Grid and time independence test was done first, and then flow past a single circular cylinder was simulated to validate the numerical model used. The comparison of current results (time-mean drag C_D, fluctuating lift C_L' and Strouhal number St) with those published in the literature states a good agreement (Table 1).

Formatted: Font: 10 pt, Italic

Table 1. Comparison of results for a single cylinder at Re = 100.

	C_D	C_L'	St
Present	1.37	0.288	0.165
[2], Exp.	--	--	0.164
[3], Exp.	--	0.18 ~ 0.54	0.168
[4], CFD	1.37	--	0.165
[5], CFD	1.36	0.287	0.166

3. Results and Discussion

Flow structures

g^* = 0, 0.25, 0.5, 0.75, 1.0, 1.25, 1.5, and 2.0 are simulated systematically. Fluid dynamics, flow structures and forces acting the cylinders are investigated at each g^*. Four distinct flow regimes are observed in the range of g^* examined.

Interlocked flow ($g^* \geq 2.0$) Four cylinders each generates a vortex street that resembles a single cylinder's street (Fig. 2a). The four streets and the shedding from the cylinders are however interlocked in an inphase fashion. The inphase flow can further be confirmed by the time-histories of lift forces of the four cylinders (Fig. 2b). The two outer cylinders (cylinders 1 and 4) have the same amplitude of lift, larger than that of the inner cylinders (cylinders 2 and 3). The time-mean value of the lift is, however, positive for the upper two (cylinders 1 and 2) and negative for the lower two (cylinders 3 and 4), implying that all the cylinders experience a repulsive lift force about the centerline $y^* = 0$ of the four cylinders. While the lift fluctuations of the two inner cylinders are exactly inphase, those of the two outer cylinders are also inphase but with a phase lag $\delta\phi = 35°$ with respect to

the inner cylinders. All the lift signals corresponded to the same St = 0.194 obtained from the power spectra of lift forces, which is ~18% higher than for an isolated cylinder.

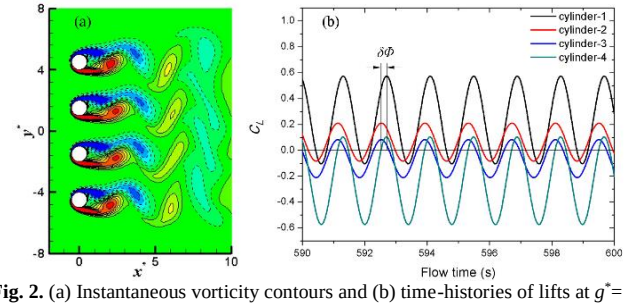

Fig. 2. (a) Instantaneous vorticity contours and (b) time-histories of lifts at g^* = 2.0.

Quasi-interlocked Flow (1.0 ≤ g*< 2.0) When g^* is decreased to 1.0 ≤ g^* < 2.0, the flow becomes chaotic. Figure 3 displays instantaneous vorticity contours and time-histories of lift forces at g^* = 1.5, demonstrating that the sheddings from the two outer cylinders, with an identical frequency, are interlocked almost inphase, and those from the other two, with another identical frequency, larger than the prior, are interlocked antiphase.

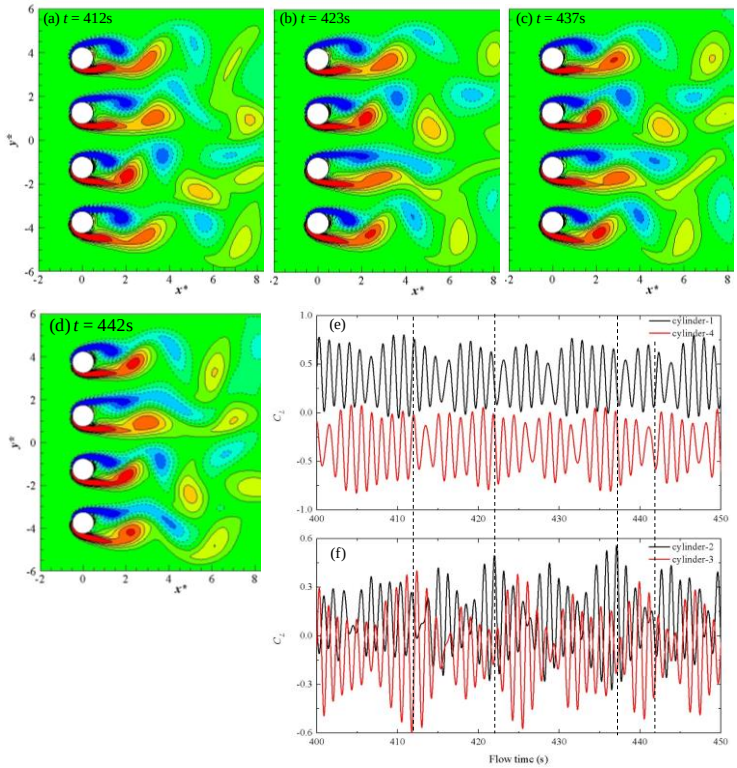

Fig. 3. (a-d) Instantaneous vorticity contours and (e, f) time-histories of lift coefficients. g^* = 1.5.

From the power spectra of the lift forces, St = 0.201 and 0.234 were estimated for the outer and inner cylinders, respectively. Due to the difference in the shedding frequencies between the outer and inner cylinders, the four cylinders may have a different instantaneous phase lag in their sheddings, e.g., inphase for the upper two

cylinders and antiphase for the lower two (Fig. 3a), and vice versa, the upper two antiphase and the lower two inphase (Fig. 3b, c). For the former pattern (Fig. 3a), the fluctuation in the lift is the greatest for cylinder 3 as the sheddings from either gap concerned with the cylinder is coupled (≈0° phase lag); it is the smallest for cylinder 2 as the sheddings are coupled from the lower gap of the cylinder and decoupled (≈180° phase lag) from the upper gap. On the other hand, for the latter pattern (Fig. 3b, c), cylinder 2 - accompanied by coupled shedding from the each of the two adjacent gaps - experiences a larger fluctuating lift (Fig. 3e, f)

Interestingly, when the sheddings from the lower two gaps or the upper two gaps are coupled and the sheddings from the other gap are of about 90° phase lag, there will be a tendency of the sheddings from the latter gap to be coupled, with the shedding from the outer side of the associated inner cylinder slowing down (e.g., cylinder 2, Fig. 3a; cylinder 3, Fig. 3b; cylinder 3, Fig. 3c; cylinder 2, Fig. 3d). In such a case, the corresponding cylinder will have a wider wake and smaller fluctuation in the lift; see the lift of the corresponding cylinder in Fig. 3(f).

The difference in frequencies also makes the time series of the lift forces have a beat-like change with varying amplitude (Fig. 3e, f). The two inner cylinders experience a larger undulation in their lifts than the two outer cylinders. This is because the two inner cylinders have the chance of coupled shedding from the two adjacent gaps. For the outer cylinders, coupled shedding may happen only from one gap concerned.

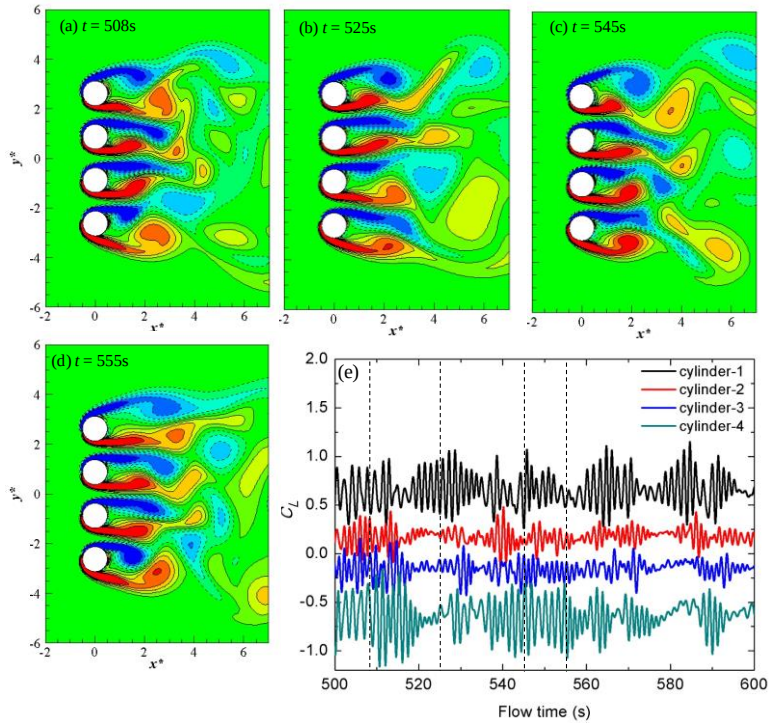

Fig. 4 (a-d) Instantaneous vorticity contours and (e) time-histories of lift coefficients. g^*= 0.75.

Flip-flopping Flow (0.25 < g*< 1.0) Wakes being narrower or wider than that of a single isolated cylinder appear behind the four cylinders when 0.25 < g^* < 1.0.The narrow and wide wakes switch from one to the other randomly as can be seen from the vorticity patterns and lift signals shown in Fig. 4 for g^* = 0.75. The two outer cylinders feature wide wakes (Fig. 4a, c), larger lift amplitudes (Fig. 4e), stronger shedding occurring alternately, coupled sheddings from the gap concerned, while the inner cylinders have opposite features: narrow wakes, smaller lift amplitudes, and weaker shedding not alternating exactly. The larger amplitude of the lift for the outer cylinders largely results from the alternate and coupled sheddings from the gaps concerned. A strong alternating shedding appearing only for cylinder 1 (Fig. 4b) and only for cylinder 4 (Fig. 4d) engenders again a large amplitude of lift of the respective cylinders. The observation implies that the outer and inner cylinders

largely undergo respectively larger and smaller lift amplitudes due to an alternating shedding for the former and almost symmetric shedding for the latter. The symmetric sheddings from the inner cylinders are more conspicuous at a smaller g^*= 0.5 (Fig. 5). Comparing Figs. 4 and 5, it can be concluded that the widths of wide and narrow wakes swell and shrink, respectively, with g^*decreasing.

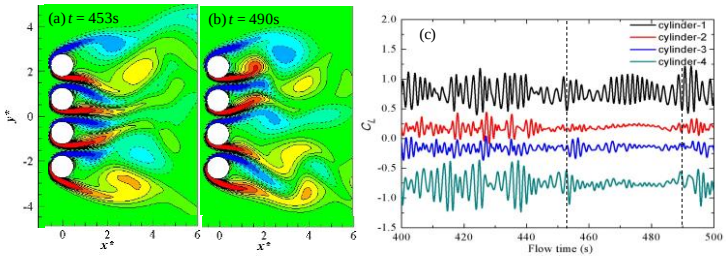

Fig. 5. (a-b) Instantaneous vorticity contours and (c) time-histories of lift coefficients. g^*= 0.5.

Single-body Flow ($g^* \leqslant 0.25$) The four cylinders act as a combined bluff body where vortex sheddings occur only from the freestream sides of the outer cylinders, forming one Karman wake of a much smaller *St* (Fig. 6a). The gap flows are too weak to form vortices and interfere the freestream side shear layers. However, they move freely up and down following the sheddings from the freestream sides. Lift histories of the four cylinders are regular and of constant amplitude and frequency. A large amplitude of lift, however, prevails for the outer cylinders. Overall, observing the lift signals, it can be concluded that time-mean lift force is always repulsive about $y^* = 0$, decreasing with increasing g^*.

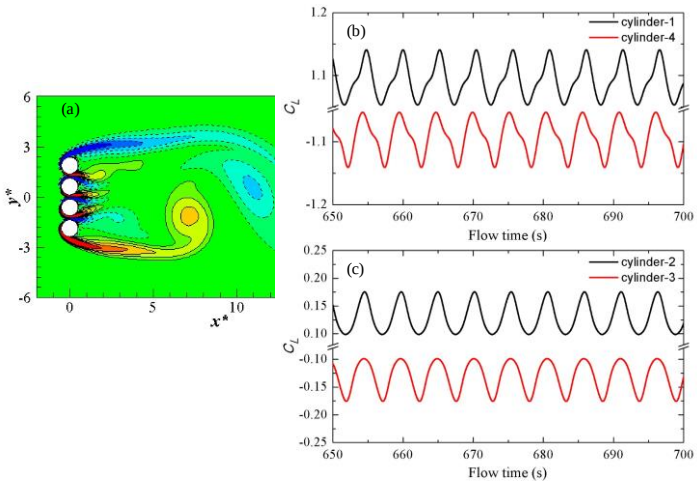

Fig. 6. (a) Instantaneous vorticity contours and (b, c) time-histories of lift coefficients. g^* = 0.25.

Total time-mean drag force

It would be interesting to know how the time-mean drag force on the four cylinders varies with g^*. The total drag force $C_{D1\text{-}4}$ on the four cylinders is obtained by adding drag forces of the individual cylinders. It is presented as $C_{D1\text{-}4}/4C_{D0}$ in Fig. 7, where C_{D0} is the drag force on a single isolated cylinder. $C_{D1\text{-}4}/4C_{D0}$ levitates with a decrease in g^* and reaches a maximum of 2.36 when the cylinders are closely connected. That is, the total drag on four cylinders (fingers) in contact is 2.36 times larger than that for a very large spacing. With a decrease in g^*, the increase in drag is dramatic ($1.68 \leq C_{D1\text{-}4}/4C_{D0} \leq 2.36$), significant ($1.4 < C_{D1\text{-}4}/4C_{D0} < 1.68$), and mild ($1.29 \leq C_{D1\text{-}4}/4C_{D0} < 1.4$) in the range $g^* \leq 0.25$, $0.25 < g^* < 1.0$ and $1.0 \leq g^* < 2.0$, respectively, corresponding to the single bluff-body, flip-flopping and quasi-interlocked flows. The relationship between $C_{D1\text{-}4}$ / $4C_{D0}$ and g^* can be represented by a best fit curve equation, coefficients obtained using least square method, as follows,

$$\frac{C_{D1\text{–}4}}{4C_{D0}} = 1.0 + 0.51e^{-0.26g^*} + 0.85e^{-6g^*}.$$

The solid line in Fig. 7 represents the above equation. When $g^* \rightarrow \infty$, the equation gives $C_{D1\text{-}4} / 4C_{D0} = 1.0$, satisfying that each of the cylinders behaves as single cylinder at a large g^*.

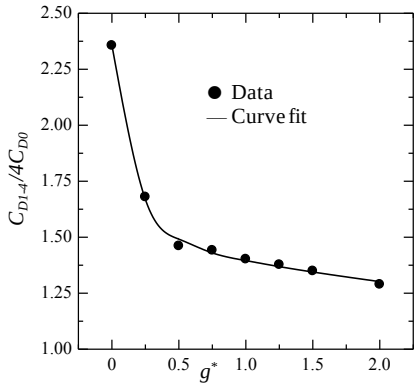

Fig. 7. Variation in the total time-mean drag on four cylinders against g^*.

4. Conclusions

A low-Reynolds number (Re = 100) flow around four side-by-side circular cylinders is investigated with a change in g^* from 0 to 2.0. Vorticity patterns, shedding frequencies and drag and lift forces are extracted and presented. Depending on g^* and features of the wake, the flow can be classified into four: single bluff-body, flip-flopping, quasi-interlocked, and interlocked flows appearing at $g^* \leq 0.25$, $0.25 < g^* < 1.0$, $1.0 \leq g^* < 2.0$, and $g^* \geq 2.0$, respectively.

The single bluff-body flow is characterized by a hefty drag force ($1.68 \leq C_{D1\text{-}4}/4C_{D0} \leq 2.36$) and a single wake behind the four cylinders. Prevailing wide and narrow wakes behind the cylinders, flip-flopping from one to the other randomly, exemplify the flip-flopping flow. The drag force is still significant ($1.4 < C_{D1\text{-}4}/4C_{D0} < 1.68$), but smaller than that in the single bluff-body flow. A further smaller drag force ($1.29 \leq C_{D1\text{-}4}/4C_{D0} < 1.4$) prevails in the quasi-interlocked flow where the sheddings from the outer cylinders are interlocked inphase and that from the inner cylinders are antiphase, with a larger shedding frequency appearing for the latter. The interlocked flow features the sheddings from all cylinders occurring in an inphase fashion with an identical frequency.

5. Acknowledgments

Alam wishes to acknowledge supports given to him from the Research Grant Council of Shenzhen Government through grant JCYJ20120613145300404.

6. References

[1] M.M. Alam, M. Moriya, and H. Sakamoto, "Aerodynamic Characteristics of Two Side-by-Side Circular Cylinders and Application of Wavelet Analysis on the Switching Phenomenon". Journal of Fluids and Structures, Vol. 18, pp. 325-346, 2003.

[2] C.H.K. Williamson, " 2-D and 3-D Aspects of the Wake of a Cylinder, and Their Relation to Wake Computations", Lectures of Applied Mathematics, Vol. 28, pp.719-751, 1991.

[3] C. Norberg, "Fluctuating Lift on a Circular Cylinder: Review and New Measurements", Journal of Fluids and Structures, Vol. 17, pp. 57–96, 2003.

[4] J.R. Meneghini, and F. Saltara, "Numerical Simulation of Flow Interference between Two Circular Cylinders in Tandem and Side-by-Side Arrangements Journal of Fluids and Structures, Vol. 15, pp.327-350, 2001.

[5] H. Ding, C. Shu, Y.O. Yeo, and D. Xu, "Numerical Simulation of Flows around Two Circular Cylinders by Mesh-Free Least Square-Based Finite Difference Methods", International Journal of Numerical Math and Fluids, Vol. 53, pp. 305–332, 2007.